Developmental Cell
Article

Fuz Mutant Mice Reveal Shared Mechanisms between Ciliopathies and FGF-Related Syndromes

Jacqueline M. Tabler,[1,6] William B. Barrell,[1] Heather L. Szabo-Rogers,[1,5,7] Christopher Healy,[1,5] Yvonne Yeung,[1] Elisa Gomez Perdiguero,[2] Christian Schulz,[2] Basil Z. Yannakoudakis,[1] Aida Mesbahi,[1] Bogdan Wlodarczyk,[3] Frederic Geissmann,[2] Richard H. Finnell,[3] John B. Wallingford,[4] and Karen J. Liu[1,*]
[1]Department of Craniofacial Development and Stem Cell Biology, Dental Institute
[2]Centre for the Cellular and Molecular Biology of Inflammation
King's College London, London SE1 9RT, UK
[3]Dell Pediatric Research Institute, Departments of Nutritional Sciences, Chemistry, and Biochemistry, The University of Texas at Austin, Austin, TX 78723, USA
[4]Howard Hughes Medical Institute and Section of Molecular Cell and Developmental Biology and Institute for Cellular and Molecular Biology, The University of Texas at Austin, Austin, TX 78712, USA
[5]These authors contributed equally to this work
[6]Present address: Section of Molecular Cell and Developmental Biology, University of Texas, Austin, TX 78712, USA
[7]Present address: Department of Oral Biology, Center for Craniofacial Regeneration, University of Pittsburgh, Pittsburgh, PA 15260, USA
*Correspondence: karen.liu@kcl.ac.uk
http://dx.doi.org/10.1016/j.devcel.2013.05.021

SUMMARY

Ciliopathies are a broad class of human disorders with craniofacial dysmorphology as a common feature. Among these is high arched palate, a condition that affects speech and quality of life. Using the ciliopathic *Fuz* mutant mouse, we find that high arched palate does not, as commonly suggested, arise from midface hypoplasia. Rather, increased neural crest expands the maxillary primordia. In *Fuz* mutants, this phenotype stems from dysregulated Gli processing, which in turn results in excessive craniofacial *Fgf8* gene expression. Accordingly, genetic reduction of *Fgf8* ameliorates the maxillary phenotypes. Similar phenotypes result from mutation of oral-facial-digital syndrome 1 (*Ofd1*), suggesting that aberrant transcription of *Fgf8* is a common feature of ciliopathies. High arched palate is also a prevalent feature of fibroblast growth factor (FGF) hyperactivation syndromes. Thus, our findings elucidate the etiology for a common craniofacial anomaly and identify links between two classes of human disease: FGF-hyperactivation syndromes and ciliopathies.

INTRODUCTION

Craniofacial dysmorphology is a common component of the ciliopathy disease spectrum, but while defective neural crest (NC) cell migration has been implicated in Bardet-Biedl Syndrome (BBS) (Tobin et al., 2008), little else is known about the underlying developmental processes in ciliopathy-associated craniofacial defects. Among the more consistent craniofacial phenotypes in ciliopathies is the presence of a high arched palate (Beales et al., 1999). In this condition, the palate is characterized by a pronounced median groove, but the roof of the mouth remains intact across the midline. This condition is often referred to as a "pseudo-cleft." Later in life, a high arched palate is also associated with secondary dental anomalies, such as postnatal gingival swelling and crowding of the molars. These defects can impair speech and complicate intubation, a major concern for craniofacial patients who frequently require multiple surgeries during childhood. Thus, high arched palate has a significant impact on patients' quality of life.

The etiology of high arched palate remains obscure. One long-held hypothesis proposes that the arch arises from a midface hypoplasia causing insufficient maxillary growth and subsequent compression of the upper dental arch (Hennekam et al., 2010; Kreiborg and Cohen, 1992; Slaney et al., 1996). However, recent morphometric analyses suggest that this may not be true (Martínez-Abadías et al., 2010). Although a chemically induced rat model has existed for several decades, the embryological progression of the phenotype is unknown (Lorente et al., 1981). Surprisingly, no genetic model of high arched palate has yet been reported, so the underlying cellular and anatomical causes remain unknown and developmental hypotheses are untested.

Clinical observations also complicate our picture of high arched palate, as this defect is associated with a variety of seemingly unrelated syndromes (Hayward et al., 2004; Hennekam et al., 2010; Kreiborg and Cohen, 1992; Vadiati Saberi and Shakoorpour, 2011). For example, though rarely mentioned in the literature, high arched palate is a central feature in many ciliopathies, including BBS, oral-facial-digital syndromes (OFD types I and IV), Joubert syndrome, and Sensenbrenner syndrome (Beales et al., 1999; Hennekam et al., 2010; Moore et al., 2005; Prattichizzo et al., 2008; Sensenbrenner et al., 1975; Somlo et al., 1993). In fact, 88% of BBS patients present with high arched palate, and many also display associated dental crowding and soft tissue swellings (Beales et al., 1999). High arched palate is also consistently observed in an array of syndromes characterized by dysregulation of fibroblast growth factor (FGF) signaling or downstream components such as the Ras kinase (Goodwin et al., 2012). Examples include Apert, Crouzon, Muenke, and cardio-facio-cutaneous syndromes (Agochukwu

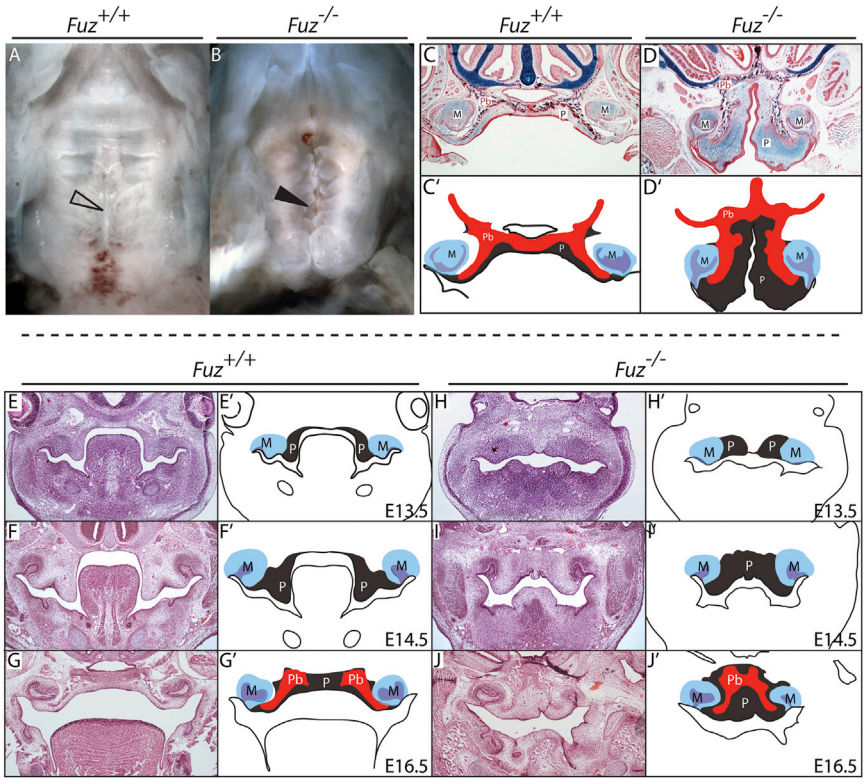

Figure 1. *Fuz* Mutant Mice Are a Model for High Arched Palate

(A and B) Ventral views of E17.5 palates. Mutants exhibit a narrow palate (arrowheads) and disrupted rugal organization compared to littermates.

(C and D) Sirius red/alcian blue staining of E17.5 coronal sections. Bilateral palatine bones are formed in both control and mutant, abutting at the midline (black). Mutant palatine bones (Pb) are mediolaterally shortened with an increase in the ventral extension. Note enlarged palatal mesenchyme (P). Molars (M) appear normal.

(C′ and D′) Schematics depicting skewed palatal anatomy.

(E–J) Hemotoxylin and eosin staining of coronal sections at indicated stages.

(E′–J′) Schematics of sections identifying palatal mesenchyme (gray, P), molars (blue and purple, M), and palatal bone condensations (red, Pb). In (H) through (J′), mutant palatal condensations are medially constrained and do not extend into the oral cavity. Palatine bone can be observed in both mutants and controls by E16.5.

See also Figure S1.

et al., 2012; Berkowitz, 1971; Hennekam et al., 2010; Kreiborg and Cohen, 1992; Letra et al., 2007; Rynearson, 2000; Vadiati Saberi and Shakoorpour, 2011). This finding is curious, because while FGF signals have been implicated in controlling cilium length (Hong and Dawid, 2009; Neugebauer et al., 2009), there has been no evidence to date suggesting a link between FGF dysregulation syndromes and the ciliopathies.

To characterize ciliopathic craniofacial defects, we examined mice with a mutation in the gene encoding *Fuzzy* (*Fuz*), which has recently emerged as a key regulator of ciliogenesis (Gray et al., 2009; Park et al., 2006). Initially described as a *Drosophila* planar cell polarity effector gene (Collier and Gubb, 1997), studies in both *Xenopus* and mice identified Fuz as a central regulator of vertebrate ciliogenesis (Brooks and Wallingford, 2012; Gray et al., 2009; Park et al., 2006). Consistent with the key role of cilia in Hedgehog (Hh) signaling, disruption of Fuz affects Hedgehog-dependent patterning events in both frogs and mice (Gray et al., 2009; Park et al., 2006), and in mice, loss of *Fuz* has been shown directly to disrupt the processing of Gli3 (Heydeck et al., 2009). Recently, live imaging analyses revealed that Fuz is essential for normal trafficking of the retrograde intraflagellar transport (IFT) machinery in vertebrate cilia; when Fuz is depleted, localization of IFT-A proteins, such as IFT43, is disrupted (Brooks and Wallingford, 2012). As a consequence, IFT trains become stalled, leading to shortened cilia and impaired signal transduction. Finally, *Fuz* is of particular interest because it is mutated in human patients with birth defects (Seo et al., 2011) and because *Fuz* mutant mice display a variety of craniofacial phenotypes (Zhang et al., 2011).

Here, we present the *Fuz* mutant mouse as a useful genetic model for the study of high arched palate. Although current hypotheses suggest that high arched palate arises from constriction of the upper jaw (Hennekam et al., 2010), our data demonstrate that the primary cause of ciliopathic high arched palate is instead excessive NC producing an enlarged first branchial arch (BA1) and maxillary hyperplasia early in embryogenesis. We have also discovered a surprising mechanistic basis for this phenotype, as we observed a dramatic increase in FGF signaling due to increased cranial *Fgf8* gene expression. Genetic reduction of *Fgf8* rescues the maxillary defects in *Fuz* mutant mice. Finally, we observed a similar maxillary expansion and upregulation of *Fgf8* expression in another ciliopathy mouse model, OFD-1 (Ferrante et al., 2006). Thus, we have identified dysregulation of FGF function as the cause of facial defects in ciliopathic mutant mice, demonstrating etiological commonalities between two broad categories of human congenital anomalies: the ciliopathies and the FGF-related syndromes.

RESULTS

Fuz Mutant Mice Are a Model of High Arched Palate

Fuz mutant mice appear to have a cleft secondary palate (Figures 1A and 1B); however, frontal sections revealed that the palatal shelves were, in fact, not clefted (Figures 1C–1D′). Instead, in all mutants analyzed, the palatine bones displayed the classic inverted-V shape typical of a high arched palate (Figures 1D–1D′). Palatal narrowing and palatine bone defects were observed throughout the anterior-posterior extent of the secondary palate in mutants (Figure S1 available online). We also observed expanded mesenchyme within the oral cavity in *Fuz* mutant mice (Figure 1D, "P" in light blue area; Figure 1D′, gray area). Thus, the maxillary phenotypes of *Fuz* mutant mice bear a striking similarity to the high arched palate reported for human ciliopathy patients (Beales et al., 1999; Hennekam et al., 2010; Tagliani et al., 2010).

The embryological events leading to high arched palate have not been previously described, so we compared maxillary development in a staged series of wild-type and *Fuz*$^{-/-}$ littermates. In controls, the palatal shelves developed bilaterally, growing and extending ventrally into the oral cavity at E13.5 (Figures 1E and 1E′). The palatal primordia were evident at the appropriate stage in *Fuz* mutants but were displaced medially compared to littermates and did not extend ventrally (Figures 1H and 1H′, outlined in gray). At E14.5, palatal condensations in controls remained bilateral and were fully extended, flanking the tongue (Figures 1F-1F′), with the palate fusing by E16.5 (Figures 1G and 1G′). In mutants, however, the palatal condensations did not extend and instead appeared as one contiguous domain (Figures 1I–1J′). This medial shift of the palatal shelves was also evident from *Patched1 (Ptc1)* expression, which spans the midline (Figure S1A and S1B). Likewise, ossification of palatine bones was apparent at E17.5 in controls, and in *Fuz* mutants the palatine bones were displaced medially (Figures 1D and 1D′). Furthermore, analysis by microcomputed tomography (μCT) revealed that the majority of midfacial bones are present and ossifying. Though small and constrained, the mutant palatine bones are roughly normal in shape (Figures S1M–S1M″). These data raised the intriguing possibility that a recognizable palate can form despite an initial failure of shelf outgrowth (Figures 1H and 1H′).

Fuz Mutant Mice Displayed Enlarged Maxillary Processes

When examined at earlier stages, we found that a larger maxillary process was evident in *Fuz* mutants as early as E9.0 (Figures 2A and 2B); by e9.5 the maxillary domain is substantially larger (compare Figures 2C and 2E to Figures 2D and 2F). Cell numbers were significantly increased in the maxilla, but there was no coincident increase in mitotic cells or change in apoptosis (Figures 2G and 2H; data not shown). Overall, this developmental progression is strikingly divergent from that underlying traditional cleft palates (Chai and Maxson, 2006), suggesting that the high arched palate, though commonly referred to as a "pseudocleft," is unrelated to cleft palate and arises by a distinct developmental mechanism.

Disruption of *Fuz* Leads to Excessive NC

We next sought to better understand the developmental origin of this defect. Because the maxillary process normally arises from NC cells emanating from the posterior mesencephalon, we lineage-traced the NC using a *Wnt1-cre* driver to follow cell migration into BA1 (Figures 2A and 2B′ blue/*lacZ*; Figures 2I–2L green/green fluorescent protein [GFP]) (Danielian et al., 1998; Muzumdar et al., 2007; Soriano, 1999). In *Fuz* mutants, we observed an early expansion of cranial NC cells (Figures 2A and 2B). In Figure 2B, the rostral extent of this expansion is marked by an asterisk. We also observed a general expansion of midhindbrain streams (Figures 2A–2B′; note brackets in Figures 2A and 2B). Most strikingly, dorsal views of these embryos revealed a substantial increase of labeled cells in BA1 and the second branchial arch (BA2) (arrowheads, Figures 2A′ and 2B′). To confirm the increase in the NC, we isolated E9.25 cranial tissues from a reporter line expressing membrane GFP (*mT/mG*) when crossed to the *Wnt1-cre* driver (schematic in Figure 2O) (Danielian et al., 1998; Muzumdar et al., 2007). Using flow cytometry, we analyzed *Wnt1-cre* induced GFP-positive cells and found a significant increase in the proportion of NC cells (summarized in Figure 2P; representative plot per genotype in Figure 2O). These experiments suggest that the observed maxillary hyperplasia may stem from an excess of NC cells.

Loss of *Fuz* Leads to Disorganized NC Migration

In addition to the significant increase in NC cell numbers, the migration of the NC was disrupted in *Fuz* mutant mice. For example, we frequently observed a large proportion of rostral crest cells collecting ectopically in the optic cup regions (Figure 2B, arrowhead). To examine this at a cellular level, we utilized membrane-bound GFP in *Wnt1-cre; R26*$^{mT/mG}$ embryos. Strikingly, three-dimensional confocal imaging revealed that the depth of the migratory streams was far greater in *Fuz* mutants (79 ± 16 μm deep in mutants versus 41 ± 20 μm deep in wild-type embryos; Figures 2K and 2L). This was surprising, as mesencephalic NC cells should remain adjacent to the epidermal ectoderm, avoiding the underlying mesenchyme (Noden, 1975). Furthermore, we noted cells rostral to the trigeminal ganglion in a region that should ordinarily be clear of NC cells (compare Figure 2I′ to Figure 2J′).

We had previously shown that morpholino oligonucleotides (MOs) were an effective means to block Fuz function in *Xenopus* (Park et al., 2006). When we examined expression of *Twist,* a migratory NC marker, following *Fuz* knockdown, we observed aberrant migration of the anterior cranial crest (Figures 2M and 2N, arrowheads), consistent with the observed craniofacial defects (Park et al., 2006). In many cases, we noted increased and ectopic migration of the anterior NC into the eye field (Figure 2N, black arrowhead and inset). Together, these data suggest that *Fuz* plays an evolutionarily conserved role in controlling NC cell contributions to BA1.

Disruption of Cranial Hedgehog Signaling at Early Stages in *Fuz* Mutant Mice

We next sought to understand the molecular basis of the maxillary hyperplasia in *Fuz* mutant mice. *Fuz* controls ciliogenesis, and cilia are central to proteolytic cleavage of Gli effector proteins that transduce Hedgehog signals (Goetz and Anderson, 2010; Liu et al., 2005; Singla and Reiter, 2006). Indeed, loss of *Fuz* leads to defective Hedgehog signaling in the spinal cord and limb (Gray et al., 2009; Heydeck et al., 2009; Park et al., 2006), and Heydeck et al. showed that, during patterning of the limb, *Fuz* mutation leads to aberrant proteolytic processing of Gli3 (Heydeck et al., 2009).

However, changes in palatal Hh signaling could not account for the observed craniofacial phenotypes, as the Hh target gene *Ptc1* continues to be expressed in *Fuz* mutant palatal primordia at E14.5 (Figures S1A–S1B′), and unlike the *Fuz* mutation, loss or gain of Hh activation in the palate leads to a true cleft rather than an arched palate (Cobourne et al., 2009; Gritli-Linde et al., 2007; Hu and Helms, 1999; Lan and Jiang, 2009; Mo et al., 1997; Rice et al., 2004). Furthermore, *Gli3* mutation also leads to sporadic cleft palate due to obstruction by the tongue (Huang et al., 2008). These data suggest that, if a Gli processing defect is involved, it must occur prior to palate formation.

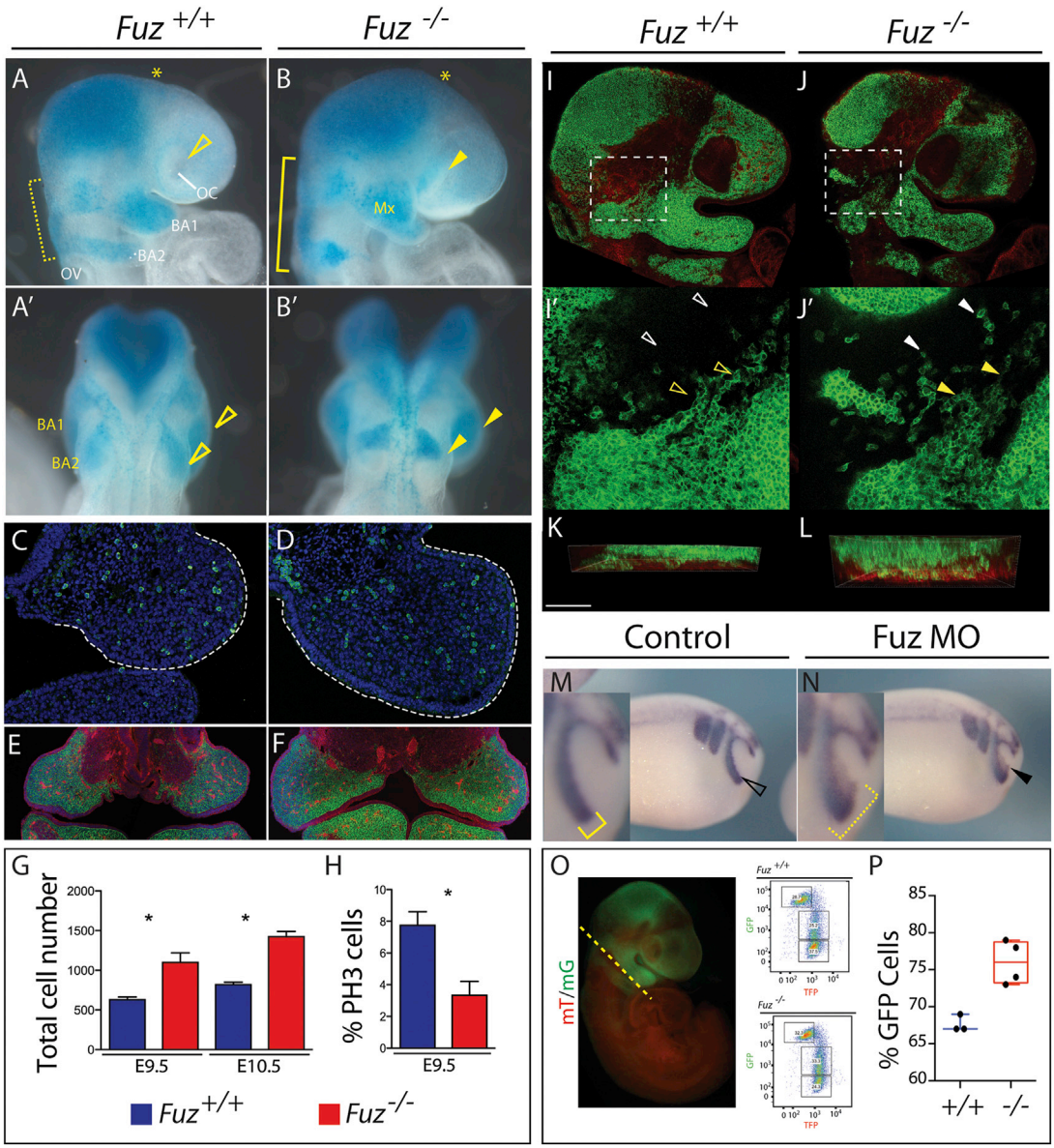

Figure 2. Increase in NC in Maxillary Compartment

Wnt1-cre-driven *LacZ* (blue) or *GFP* (green) marks NC contributions.

(A and B) Lateral views of E9.25 embryos. BA1 and BA2 NC streams are wider compared to controls (B compared to A, yellow bracket). Increased NC disrupts the optic cup (OC) in *Fuz* mutants compared to controls (B compared to A, arrowhead). BA2 NC stream is also increased in size and has failed to migrate as far as BA2 control NC. Mx, maxillary compartment of BA1. OV, optic vesicle.

(A′ and B′) Dorsal views. Maxillary BA1 is enlarged compared to controls (B compared to A, top arrowhead). BA2 has failed to migrate sufficiently compared to controls (bottom arrowhead).

(C and D) PH3 staining (green) and DAPI (blue) of E9.0, maxillary compartment. Mutant maxilla is enlarged (white dotted line).

(E and F) Coronal sections of E10.5 *Wnt1-cre; R26R*$^{mT/mG}$; *Fuz*$^{+/+}$, or *Wnt1-cre; R26R*$^{mT/mG}$;*Fuz*$^{-/-}$ maxillae. *Wnt1-cre*-driven membrane-GFP (green) marks NC contributions. Epithelial membrane-Tomato (red) highlights all other tissue derivatives. Mutant maxillae are larger compared to controls. Enlarged maxillae comprise NC-derived mesenchyme.

(G) Quantification of DAPI-positive cells from representative sections of E9.5 and 10.5 embryos. Note increase in cell number in mutant (red) maxilla compared to wild-type (blue) ($p < 0.004$). Error bars indicate SD.

(H) Quantification of E9.5 maxillary PH3-positive cells compared to total cell number. A significant decrease in the percentage of PH3-positive cells is observed in mutant maxillae (red) compared to controls (blue) ($p < 0.01$). Error bars indicate SD.

(I and J) Single confocal z-sections of *Wnt1-cre; R26R*$^{mT/mG}$;*Fuz*$^{+/+}$ or *Wnt1-cre; R26R*$^{mT/mG}$;*Fuz*$^{-/-}$ E9.5 embryos. *Wnt1-cre*-driven membrane-GFP (green) marks NC contributions.

(I′–J′) Magnified maximum projections of (I) and (J), indicated by a white dotted box. In controls, chains of *Wnt1-cre*-driven membrane-GFP-positive NC are observed (yellow arrowheads), with few isolated cells between brain and maxillary compartment (white arrowheads). Isolated NC cells are observed in mutant embryos, indicated by a white arrowhead in (J′), and NC chains are disorganized.

(legend continued on next page)

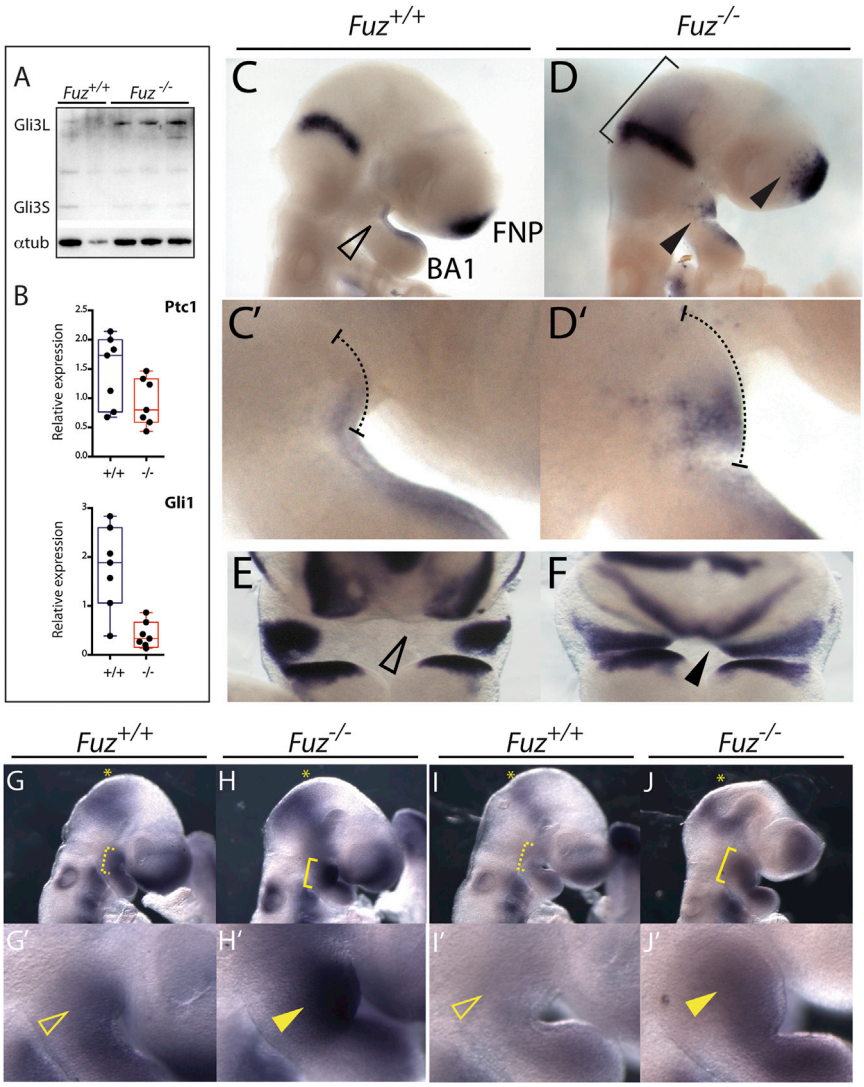

Figure 3. Gli3 Processing and Hh and FGF Signaling Are Altered in *Fuz* Mutants

(A) Western blot analysis of activator and repressor forms of Gli3 (Gli3-L and Gli3-S, respectively) in E9.0 embryos. Increased Gli3-L and reduced Gli3-S was detected in $Fuz^{-/-}$ embryos in (A), lanes 3–5, compared to controls in (A), lanes 1 and 2. Alpha-tubulin was analyzed as a loading control.

(B) qPCR of Hh target genes *Patched 1 (Ptc1)* and *Gli1* from E9.0 $Fuz^{+/+}$ and $Fuz^{-/-}$ heads. Relative mRNA levels are normalized to *β-actin*. *Ptc1* and *Gli1* are decreased in mutants (red) compared to controls (blue). Whiskers represent maximum/minimum data values with median and quartiles represented in the box.

(C and D) Lateral views of *Fgf8* expression in E9.0 embryos. *Fgf8* is expressed in the midhindbrain boundary (MHB), frontonasal prominence (FNP), and the BA1 epithelium. In mutants, *Fgf8* expression domains are expanded, indicated by bracket and arrowheads.

(C′ and D′) Magnified view of BA1 in control and mutant embryos. Dotted line indicates extent of maxillary compartment. Note enlarged maxillary prominence.

(E and F) Frontal view of *Fgf8* expression in E10.5 embryos. Note mediolateral expansion of maxillary *Fgf8* expression in the mutant, indicated by black arrowhead.

(G and H) Lateral views of *Erm1* mRNA expression in E9.5 embryos. *Erm1* is expressed in the MHB, FNP, and BA1. In mutants, expression of *Erm1* is expanded ventrally from the MHB (yellow asterisk) and in BA1 (yellow bracket).

(G′ and H′) Magnified view of BA1. *Erm1* expression is increased in mutant maxillae (yellow arrowheads).

(I and J) Lateral views of *Pea3* expression in E9.5 embryos. *Pea3* is expressed in the MHB, FNP, and BA1. In mutants, expression of *Pea3* is expanded in BA1 (yellow bracket).

(I′ and J′) Magnified view of BA1 in control and mutant embryos. *Pea3* expression is increased in mutant maxillae (yellow arrowhead).

See also Figure S2.

As it happens, Gli3 plays a crucial role in patterning the tissues that give rise to NC destined for BA1 (Blaess et al., 2006). Therefore, we assessed Hh signaling in the cranial regions of e9.0 embryos. We found a dramatic increase of full-length Gli3 in our mutants and a concurrent decrease in the short repressor form of Gli3 (Figure 3A). We also observed a reduction of Hh target gene expression in cranial tissues (Figure 3B), which may contribute to the observed NC defect.

Expanded FGF Expression in *Fuz* Mutants

We then considered molecular changes downstream of the early Gli processing defects in $Fuz^{-/-}$ mice. One possibility was that

(K and L) Z-projections of (I′) and (J′). The thickness of NC streams anterior to the prospective trigeminal ganglion is increased in mutants (WT = 41 ± 20 μm thick; mutant = 79 ± 16 μm deep). The immediately underlying membrane-Tomato-positive mesenchymal cells are shown in red, at the bottom of the image. The overlying epithelium is not included. Scale bar, 100 μm. This doubling in thickness is consistent with increased NC invasion into BA1.

(M and N) *Twist* in situ hybridization of stage 22 embryos injected unilaterally with *Fuz* MO. In controls, *Twist* is expressed in three streams, where the anterior NC stream surrounds the optic placode, indicated in (M) by open arrowhead and inset (bracket). Ectopic *Twist* expression is observed in the optic placode in Fuz morphants, indicated in (N) by arrowhead and inset (bracket).

(O) Representative epifluorescence image of an E9 *Wnt1-cre; R26*$^{mT/mG}$ embryo. Lineage-traced NC cells are labeled GFP (green), and nonrecombined cells are Tomato positive (red). Dashed line illustrates where embryos were bisected caudal to BA1. *Wnt1-cre; R26R*$^{mT/mG}$; $Fuz^{+/+}$, or *Wnt1-cre; R26R*$^{mT/mG}$;$Fuz^{-/-}$ embryo heads were dissociated and GFP positive, Tomato, or double-labeled cells were analyzed by flow cytometry. Representative flow cytometry plots from single E9 *Wnt1-cre; R26*$^{mT/mG}$; $Fuz^{+/+}$, or *Wnt1-cre; R26R*$^{mT/mG}$;$Fuz^{-/-}$ dissociated heads. mG, *Wnt1-cre*-driven membrane-GFP; mT, membrane-Tomato.

(P) The percentage of *Wnt1-Cre*-driven GFP-positive cells was significantly increased in mutants (79% ± 2%) compared to controls (68% ± 1%) ($p = 0.0103$). Whiskers represent maximum/minimum data values with median and quartiles represented in the box.

loss of *Fuz* leads to upregulation of Wnt target genes (e.g., Zhang et al., 2011); however, we found no changes in levels of activated β-catenin at early stages (e9.0) in $Fuz^{-/-}$ heads (data not shown). Next, as mentioned, high arched palate is common in FGF hyperactivation syndromes (Hajihosseini et al., 2001; Itoh and Ornitz, 2011; Wilkie et al., 1995). While there is no link between cilia and FGF signal transduction per se, loss of Gli3 can lead to increased *Fgf8* gene transcription, most obviously in the telencephalon (Aoto et al., 2002; Blaess et al., 2006; Cordero et al., 2004; Kuschel et al., 2003; Okada et al., 2008; Rash and Grove, 2007; Theil et al., 1999; Ueta et al., 2008). Indeed, a recent report suggests that loss of cilia-dependent signaling can similarly result in *Fgf8* expansion during development of the corpus callosum (Benadiba et al., 2012).

Therefore, we examined *Fgf8* levels in *Fuz* mutants. Strikingly, at E9.5, *Fgf8* expression was significantly expanded in *Fuz* mutants (Figures 3D and 3F), though there was minimal difference in mRNA levels prior to e9.0 (Figure S2). *Fgf8* is normally expressed in the midhindbrain boundary, the frontonasal process, and at low levels within the lateral epithelium of the maxillo-mandibular cleft (Figures 3C and 3C′). In *Fuz* mutants, *Fgf8* expression was expanded in all of these domains, with an anterior expansion from the midhindbrain domain (Figure 3D, bracket) and a mediolateral expansion within the mandibular and maxillary prominences (Figures 3D and 3D′). This expansion was maintained in mutant maxilla at E10.5 (Figure 3F). In addition, we found that *Fuz* knockdown in *Xenopus* also resulted in broader *Fgf8* gene expression, most strikingly in the domain abutting the migratory NC and in the frontal midline (Figure S3).

Key transcriptional targets of FGF signaling, *Erm1* and *Pea3* (Firnberg and Neubüser, 2002; Raible and Brand, 2001; Roehl and Nüsslein-Volhard, 2001), were strongly upregulated in *Fuz* mutants (Figures 3I–3J′) including a clear rostral expansion of both messenger RNAs (mRNAs) surrounding the mesencephalon (Figures 3G–3J, asterisk). Furthermore, both genes were robustly expressed throughout the expanded maxillary primordia, in contrast to the wild-type littermates (Figures 5H′ and 5J′, arrowhead). Together, these data identify a surprising role for *Fuz* in the regulation of *Fgf8* gene expression, and suggest that an aberrant increase in FGF signaling underlies the craniofacial anomalies in *Fuz* mutant mice.

Fgf8 Heterozygosity Rescues Maxillary Hyperplasia and Palate Defects in *Fuz* Mutant Mice

Our analysis of *Fuz* mutants suggested that excessive FGF signals drive the maxillary hyperplasia that underlies the observed palate defects. To test this model directly, we asked if decreasing the *Fgf8* gene dose might ameliorate the craniofacial defects in *Fuz* mutants. Using a null allele of *Fgf8*, in which the coding region is replaced with the *lacZ* gene (Ilagan et al., 2006), we halved the dose of *Fgf8* in $Fuz^{-/-}$ mice. We observed substantial rescue of maxillary hyperplasia in $Fuz^{-/-}$; $Fgf8^{lacZ/+}$ compound mutants (compare *Fuz* mutants in Figures 4B and 4B′ to rescued embryos in Figures 4C and 4C′). Heterozygosity of *Fgf8* also rescued the brain overgrowth and ocular phenotypes observed in *Fuz* mutants (compare Figure 4E to Figure 4F). Most strikingly, loss of one allele of *Fgf8* restored the e16.5 $Fuz^{-/-}$ palate to a normal width (Figures 4H–4K; Figure S3), confirming that the early maxillary phenotype is due in large part to an increase in FGF.

Because the *Fgf8* and NC phenotypes we observed seemed localized to the cranial structures, we hypothesized that phenotypic rescue after decreasing *Fgf8* dose should be specific to the head. Indeed, we found that *Fgf8* heterozygosity had little effect on digit development phenotypes in *Fuz* mutant mice (Figure S3). Together, these data suggest that the proximate cause for craniofacial defects in *Fuz* mutant mice is expanded *Fgf8* expression, while the polydactyly is independent of *Fgf8*, resulting directly from aberrant cilia-mediated Gli3 regulation (Heydeck et al., 2009).

Conditional Disruption of *Fuz* in the NC Does Not Result in High Arched Palate

Our data so far lead us to propose a model in which early dysregulation of cranial Gli processing in *Fuz* mutant mice leads to excessive expression of *Fgf8*, which in turn causes an excess of NC. We further propose that it is this early excess of NC, rather than attendant crest migration defects, that results in maxillary hyperplasia and high arched palate. To test this model, we used the NC-specific *Wnt1-cre* driver to conditionally delete the *Fuz* gene. Notably, specific deletion of *Fuz* in NC cells did not elicit early hyperplasia of the maxillary process or high arched palate (Figure 5; data not shown). Instead, these animals had a true cleft, indicating that, in the NC, *Fuz* is required only much later for palatal shelf elevation or depression of the tongue. These data suggest that the early maxillary phenotypes in *Fuz* mutant mice result from Fuz requirements in the neural tissue prior to NC induction (see also the model, Figure 7).

Maxillary Hyperplasia and FGF8 Upregulation in OFD-1 Mice

We next asked if *Fgf8* misregulation might be a general principle in ciliopathies. We examined the mouse model of OFD syndrome, *Ofd-1* (Ferrante et al., 2006). OFD patients frequently present with high arched palate (Figure 6F) (Hennekam et al., 2010; Prattichizzo et al., 2008; Tagliani et al., 2010), and OFD-1 is essential for ciliogenesis and centriole morphology (Ferrante et al., 2006; Singla et al., 2010). Importantly, *Ofd-1* mutant animals were strikingly similar to the $Fuz^{-/-}$ animals, with an enormously enlarged maxillary process and a clear expansion of cranial *Fgf8* expression (Figures 6A–6D).

Broad Similarity between *Fuz* Mutant Mice and FGF Hyperactivation Syndromes

Finally, the similarity of palatal phenotypes between OFD patients and patients with FGF hyperactivation syndromes such as Apert (Figures 6E–6G) suggest that ciliopathic cranial phenotypes stem from excessive FGF signaling. If this were the case, we hypothesized that $Fuz^{-/-}$ mice might also display craniosynostosis, another common feature of FGF hyperactivation syndromes. Therefore, we examined skull ossification using Alizarin red staining and found complete synostosis of the coronal sutures in *Fuz* mutant mice, akin to that seen in Apert syndrome (Figures 6I–6I′, arrowhead). Mutants also displayed other hallmarks of FGF syndromes, including fusion of the cervical vertebra and upper airway anomalies (data not

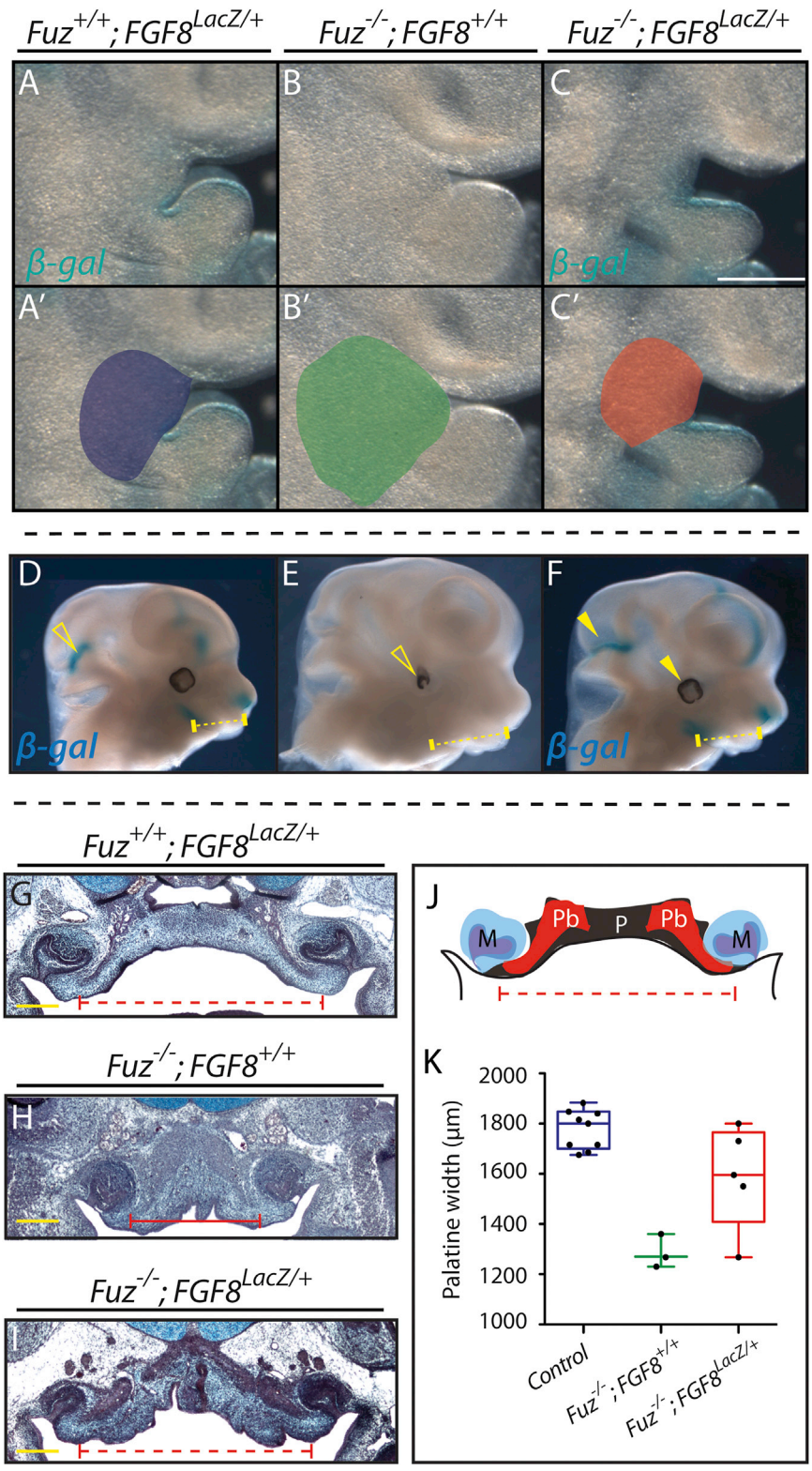

Figure 4. *Fgf8* Reduction Rescues Maxillary Hyperplasia and Palatal Width in Compound Mutants

(A–C) Lateral views of BA1. Maxillary size is expanded in $Fuz^{-/-}$ mutants in (B) compared to $Fgf8^{LacZ/+}$ in (A). Maxillary expansion is rescued in $Fuz^{-/-}$; $Fgf8^{LacZ/+}$ embryos in (C). *Fgf8* expression is also rescued in compound mutants as β-gal staining reveals similar BA1 epithelial expression in compound mutants and *Fgf8* heterozygotes.

(A′–C′) Maxillary size is schematized for each genotype.

(D–F) Lateral view, E12.5. Maxillary size is expanded in mutants in (E) compared to $Fgf8^{LacZ/+}$ in (D). Maxillary expansion is rescued in $Fuz^{-/-}$; $Fgf8^{LacZ/+}$ embryos in (F). Normal *Fgf8* expression (β-gal/blue) is also restored in compound mutants. Brain overgrowth and eye defects are rescued in compound mutants (arrowheads).

(G–I) Trichrome staining of coronal sections of E16.5 embryos. Palatal width and bone angle are decreased in mutant embryos in (H) compared to controls in (G). Palatal width in $Fuz^{-/-}$; $Fgf8^{LacZ/+}$ in (I) appears normal compared to controls in (H). Angle of palatine bone is partially rescued when compared to controls, as shown in (I) compared to (G) and (H).

(J) Schematic of palatal anatomy.

(K) Quantification of palatal width in E16.5 $Fuz^{+/+}$; $Fgf8^{LacZ/+}$(blue), $Fuz^{-/-}$; $Fgf8^{+/+}$ (green), and $Fuz^{-/-}$; $Fgf8^{LacZ/+}$(red) embryos. Palatal width is significantly decreased in $Fuz^{-/-}$; $Fgf8^{+/+}$ compared to controls, while *Fgf8* heterozygosity rescues palatal width in *Fuz* mutants ($p < 0.0005$, one-way analysis of variance). Whiskers represent maximum/minimum data values with median and quartiles represented in the box.

See also Figure S3.

shown) (Anderson et al., 1997; Kreiborg et al., 1992; Moore et al., 1995). Thus, our data suggest widespread commonalities between ciliopathic craniofacial defects and FGF hyperactivation syndromes.

DISCUSSION

Recent evidence reveals significant roles for cilia in human development and disease. First, mutations in genes known to promote cilia biogenesis and IFT have been implicated in a number of human syndromes (Ferkol and Leigh, 2012). Second, analysis of animal models suggests that a variety of developmental disorders, including craniofacial dysmorphology, result from defects in ciliary function (Huber and Cormier-Daire, 2012). Finally, advances in clinical genomics have improved annotation of disease alleles, subsequently identifying numerous, unclassified syndromes as ciliopathies (Brugmann et al., 2010). The challenge now is understanding how these seemingly heterogeneous disorders arise (Novarino et al., 2011), and our data suggest that commonalities in phenotype are likely to reflect shared signaling events, which converge into shared phenotypes. The results reveal an association between ciliopathies

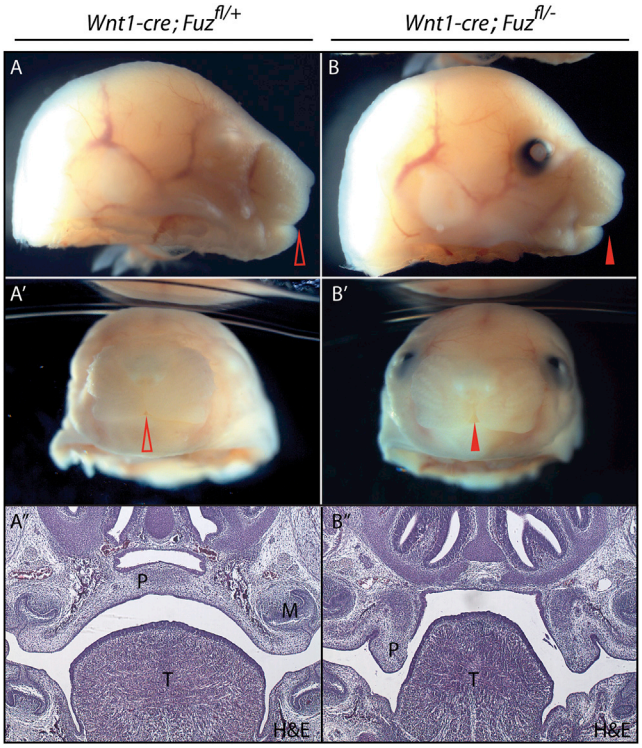

Figure 5. Maxillary Hyperplasia Is Not Due to *Fuz* Function in the NC

(A and B) Lateral views of E17.5 *Wnt1-cre; Fuz*$^{fl/+}$ and *Wnt1-cre; Fuz*$^{fl/-}$ embryos. The control embryo in (A) is an albino and lacks pigment in the eye. Arrowheads indicate rostral midline.

(A′ and B′) Frontal views of E17.5 *Wnt1-cre; Fuz*$^{fl/+}$ and *Wnt1-cre; Fuz*$^{fl/-}$ embryos. A cleft lip is observed in conditional null embryos [(B′) compared to (A′), indicated by arrowheads].

(A″ and B″) Hemotoxylin and eosin (H&E) staining of coronal sections of E17.5 *Wnt1-cre; Fuz*$^{fl/+}$ and *Wnt1-cre; Fuz*$^{fl/-}$ embryos. Sections show the anterior secondary palate (P), tongue (T), and molars (M). Palatal shelves are elevated and fused across the midline in control embryos; however, a failure in shelf elevation is observed in *Wnt1-cre; Fuz*$^{fl/-}$ embryos [(B″) compared to (A″), indicated by P]. The tongue also appears smaller and irregularly shaped in mutants [(B″) compared to (A″) indicated by T].

and FGF syndromes, in turn providing insights into the diversity of phenotypes seen in craniofacial anomalies.

We present the *Fuz* mutant as a genetic model of ciliopathic high arched palate and provide experimental evidence of the causes of this defect (Figure 7). Some aspects of skeletal development in *Fuz* mutants have been previously described; however, those reports focus on mandibular outgrowth (Zhang et al., 2011). We propose that the high arched palate arises due to perturbation of facial development in the *Fuz* mutant well before the stages examined previously and that the reported effects on Hh and Wnt signaling are secondary to an earlier developmental defect (Zhang et al., 2011).

Our data suggest that early expansion in *Fgf* gene expression drives maxillary phenotypes in the *Fuz* mutant model (Figure 7), but how does loss of a ciliopathy gene lead to an expansion of FGF signaling? In wild-type embryos, Gli3 repressor is expressed in the midbrain, where it acts as a transcriptional repressor, and indeed, Gli3R normally suppresses *Fgf8* expression in neural tissues, as loss of Gli3 leads to an increase in *Fgf8* (Aoto et al., 2002). Gli3 processing from Gli3-A (activator) to Gli3-R (repressor) is thought to occur at the distal tip of the cilium (Figure 7A) (Endoh-Yamagami et al., 2009; Lai et al., 2011; Tukachinsky et al., 2010; Wen et al., 2010). This distal tip of the ciliary axoneme is specifically lost in the absence of Fuz (Brooks and Wallingford, 2012) and likely leads to attenuated Gli3 processing (Figure 3). Subsequently, loss of Gli3R reduces transcriptional inhibition, permitting expansion of hindbrain fates, and *Fgf8* expression.

Previous studies in chicken embryos have implicated brain-specific *Fgf8* in the control of NC numbers (Creuzet et al., 2004). How does this occur? DiI labeling has shown that, in mouse, anterior NC destined for BA1 arises from the posterior mesencephalon and rhombomere 1 (Osumi-Yamashita et al., 1994). Loss of Hh activity leads to dorsalization or expansion of these structures (Fedtsova and Turner, 2001), concurrently increasing *Fgf8* expression and the NC domain. As a consequence, increased numbers of NC cells migrate toward BA1, overfilling it and forming enlarged maxillae (Figures 2 and 3). Subsequently, *Fgf8* is also upregulated in the BA1 epithelium, as well as in the frontonasal prominence (Figure 3). Following NC migration, the palatal condensation (Figure 7, red) arises medially, adjacent to *Fgf8* expression domains; in mutants, the grossly enlarged maxillary region causes a medial shift in palatal condensations (Figure 7).

These findings are significant for exposing an etiological link between the ciliopathies and FGF hyperactivation disorders. Furthermore, our data suggest that the long-held midface hypoplasia model for high arched palate should be revisited (Hayward et al., 2004; Hennekam et al., 2010). One source of confusion may be the disparity between observations in human patients versus phenotypes associated with mouse models. For example, Snyder-Warwick and colleagues examine palatal development in mice carrying a Crouzon mutation (FGFR2^{C342Y}), which causes increased FGF signaling associated with craniosynostosis (Snyder-Warwick et al., 2010). In these mice, heterozygotes, which should mirror the human genotype, have normal palates. Furthermore, homozygotes have a true cleft, mimicking a loss of FGFR2b (Hosokawa et al., 2009; Rice et al., 2004). This clearly does not model the oral aspects of the human syndrome, as it was noted nearly 40 years ago that true clefts in Crouzon patients were likely to be misdiagnoses (Peterson and Pruzansky, 1974).

Importantly, the relationship between ciliopathy and FGF hyperactivation syndromes is not limited to the palate, as *Fuz* mutant mice also display other manifestations of the FGFR-associated syndromes, such as craniosynostoses, fusions of the cervical vertebrae, and tracheal cartilaginous sleeve (Figure 6; data not shown). Finally, we note that this relationship is not restricted to animal models, as high arched palate and synostoses also co-occur in the human ciliopathy Sensenbrenner syndrome (Levin et al., 1977; Sensenbrenner et al., 1975). Notably, the cilia defects in Sensenbrenner syndrome are caused by mutations in proteins of the retrograde IFT particle, including IFT43 (Arts et al., 2011), and we recently showed that ciliogenesis defects following disruption of *Fuz* stem from a failure of IFT43 trafficking (Brooks and Wallingford, 2012).

Thus, in summary, our studies of a high arched palate model have revealed that excessive *FGF* transcription and increased

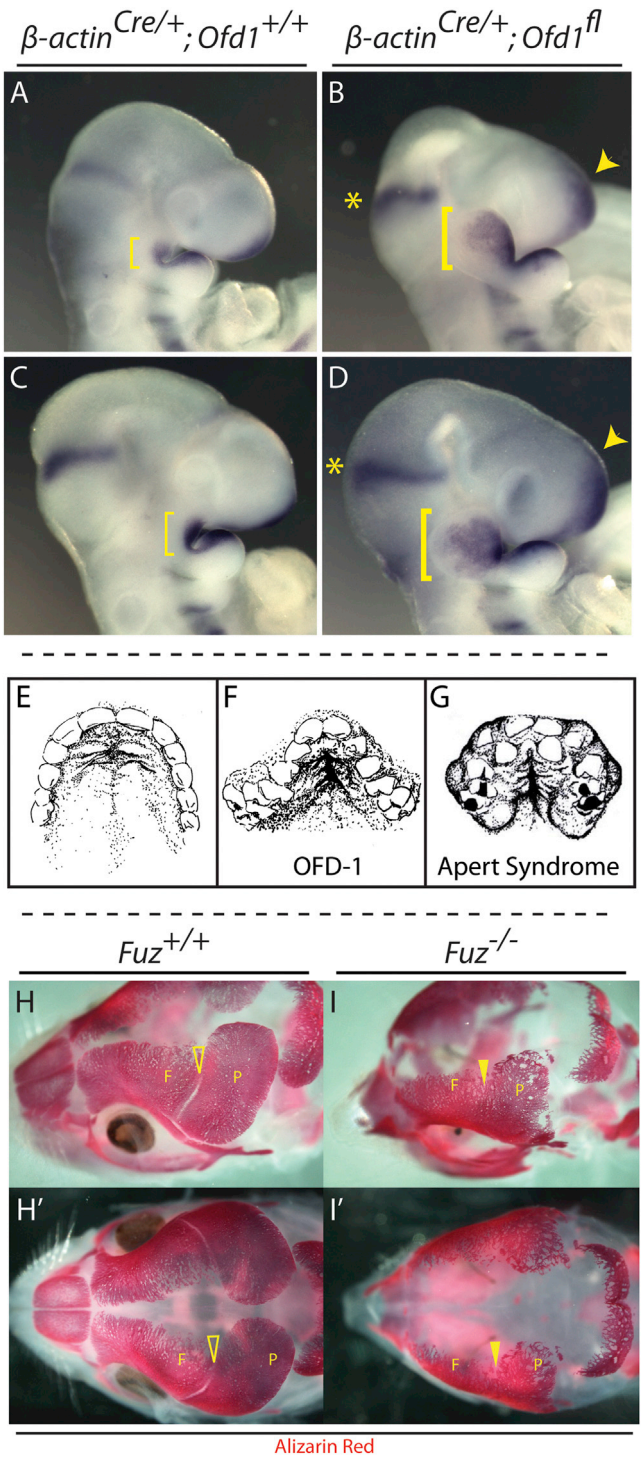

Figure 6. *Ofd-1* Mutants Also Show Expanded Maxillary Compartments and Cranial FGF8 Expression Domains

(A–D) Lateral views of E9.5 embryos showing cranial *Fgf8* mRNA expression domains. The 21 and 23 somite *ofd-1* mutants have enlarged maxillae compared to stage-matched control embryos, indicated by yellow brackets in (B) and (D) compared to (A) and (C), respectively. Maxillary *Fgf8* expression is expanded in mutants compared to controls [brackets in (B) and (D) compared to (A) and (C), as well as expression in the frontonasal process, indicated by arrowheads].

NC may be key factors in the poorly understood etiology of ciliopathic craniofacial defects. Furthermore, our report demonstrates that the pathological events underlying this phenotype are surprisingly different from those leading to a traditional cleft palate, raising the possibility that clinical diagnoses and management of high arched palate should also be reconsidered in this developmental and molecular context.

EXPERIMENTAL PROCEDURES

Mouse Lines

The following mouse lines were used: *Fuz* mutants: $Fuz^{gt(neo)}$ (Gray et al., 2009); conditional *Fuz* mutants: $Fuz^{fl/fl}$, which were generated according to standard methods and will be described elsewhere; conditional *Ofd-1* mutants: $Ofd1^{tm2.1Bfra}$ (Ferrante et al., 2006); *Fgf8* mutants: $Fgf8^{lacZ}$ (Ilagan et al., 2006); *Wnt1-cre* driver: *Tg(Wnt1-cre)11Rth* (Danielian et al., 1998); and reporter lines: $R26R^{mT/mG}$: $GT(Rosa)26Sor^{tm4(ACTB-tdTomato-EGFP)Luo}$ (Muzumdar et al., 2007) and $R26R^{lacZ}$: $Gt(ROSA)26Sor^{tm1Sor}$ (Soriano, 1999). Genotyping was performed as described in the original publications cited earlier. In all phenotypes depicted, at least four animals per genotype were examined. All animal work was performed in accordance with UK Home Office Regulations.

Western Blotting

Tissues rostral to and including BA1 were dissected from E9.0 embryos. Protein preparations and western blotting were carried out according to established protocols. Primary antibodies used were anti-Gli3 (clone H-280, 1:1,000, Santa Cruz Biotechnology no. sc-20688) and anti-alpha tubulin (clone DM1a, 1:5,000, Sigma T6199). Chemiluminescent signal was visualized using a BioRad ChemiDoc.

Real-Time PCR

Tissues rostral to and including BA1 were dissected from E9.0 embryos. Reverse transcription and cDNA synthesis were carried out according to standard protocols. Real-time PCR (RT-PCR) reactions were performed on a Rotorgene Q 2-series using the following gene-specific primer pairs.

β-actin (F: CTAAGGCCAACCGTGAAAG, R: ACCAGAGGCATACAGGGACA)
Gli1 (F: CAGGGAAGAGAGCAGACTGAC, R: CGCTGCTGCAAGAGACT)
Patched1 (F: AAGCCGACTACATGCCAGAG, R: AAGGGAACTGAGCGTACTCG)
Fgf8 (F: AGGTCTCTACATCTGCATGAAC, R: TGTTCTCCAGCACGATCTCT)
Erm (F: TGCCCACTTCATCGCCTGGAC, R: TAGCGGAGAGAGCGGCTCAG)

Staining and Histology

All mRNA in situ hybridization, immunohistochemistry, β-gal activity, and histological staining were performed according to standard protocols. Mouse

(E–G) OFD-1 and Apert syndrome patients exhibit high arched palate. In (E), a ventral view of a normal palate shows a hard palate with shallow, anterior bilateral rugae and smooth posterior palate (after photo by Millicent Odunze: http://plasticsurgery.about.com/od/Cleft-Lip-And-Palate/ss/What-Is-A-Cleft-Palate_3.htm). In (F), a ventral view is shown of the palate from OFD 1 (OFD-1) patient (after Tagliani et al., 2010; Figure 2F). (G) shows a ventral view of palate from the Apert syndrome patient (after Rynearson, 2000). Both (F) ciliopathic and (G) FGF-related high arched palates are narrow with a deep medial cleft extending from the anterior hard palate. Rugal-like swellings are more numerous and are extant with the medial cleft. Soft tissue swellings and dental crowding are observed in both groups.
(H–I′) Loss of Fuz causes coronal craniosynostosis. E17.5 heads stained with Alizarin red. (H) and (I) show dorsolateral views. (H′) and (I′) show dorsal views. Alizarin red negative coronal suture (open arrowheads) separates frontal (F) and parietal (P) bones in wild-type embryos. Coronal suture is absent in mutant embryos (closed arrowheads).

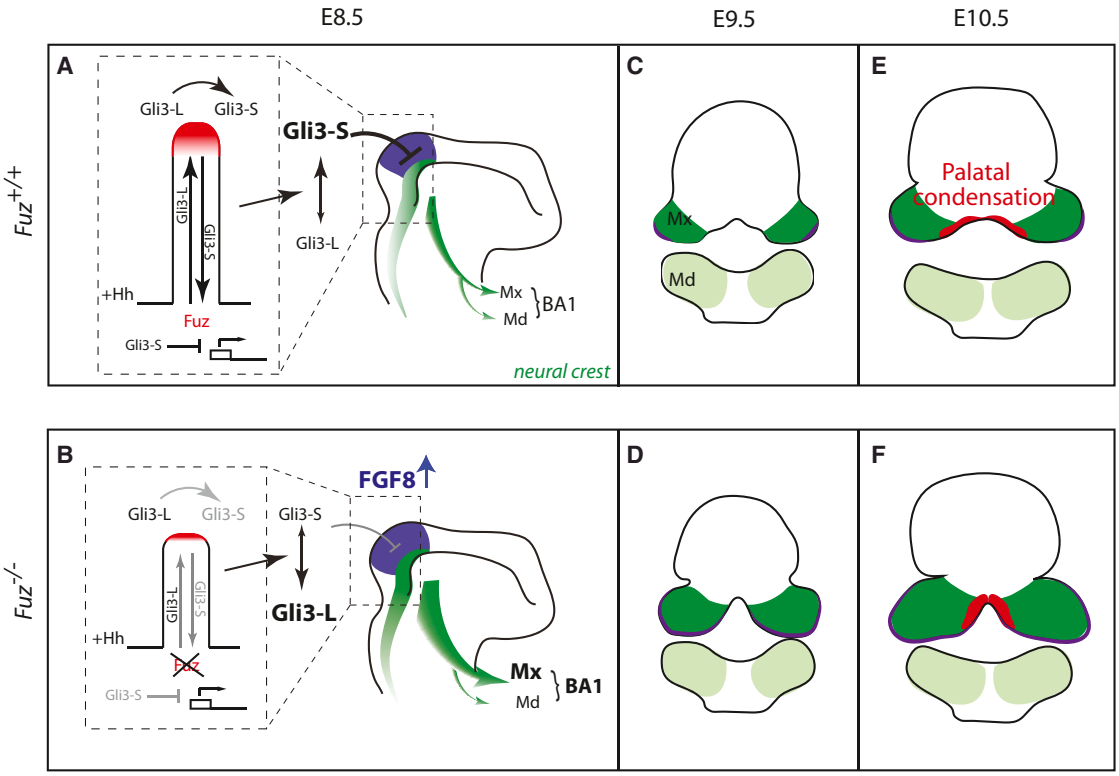

Figure 7. Proposed Model for Palatal Defects in *Fuz* Mutants

(A and B) Schematics depict E8.5 embryos. In Hedgehog signaling, anterograde transport delivers Gli3L (Gli3-activator) to the distal CLAMP-positive ciliary tip (red). Gli3-L is processed into Gli3-S (Gli3 repressor) which undergoes retrograde transport, repressing transcription of targets such as *FGF8*. Anterior NC (dark green) arises from the posterior mesencephalon and anterior hindbrain (purple), and is normally limited by a balance of Hh and FGF signals. NC then migrates into BA1, comprising maxillary and mandibular compartments (Mx and Md, respectively). When Fuz function is lost, ciliary transport and the distal compartment are severely disrupted leading to disruption of Gli processing and an expansion in cranial NC numbers, specifically maxillary NC.

(C–F) In (C) and (D), schematics depict coronal sections of E9.5 embryos. In coronal sections, the maxilla forms as two bilateral prominences and *Fgf8* is expressed in lateral maxillary epithelia, indicated by purple in (C) through (F). In mutants, the maxillary compartment is enlarged and epithelial *Fgf8* is expanded. In (E) and (F), schematics depict coronal sections of E10.5 embryos. Palatal condensations (red) are medial to *FGF8* expression domains. In wild-type animals, these flank midline mesenchyme but remain separated. In *Fuz* mutants, expansion of *FGF8* causes a medial shift of the palatal condensations. Subsequently, the normal bilateral palatal primordia join at the midline.

and *Xenopus* embryos were collected in cold PBS and fixed overnight in 4% paraformaldehyde or MEMFA, respectively. mRNA in situ hybridization was performed as previously described (Sive et al., 2000; Wilkinson et al., 1989). The following mRNA probes were used: mouse *Fgf8* (Mahmood et al., 1995), mouse *erm* (Hippenmeyer et al., 2002), mouse *Pea3* (Livet et al., 2002), *X. laevis Fgf8* (Monsoro-Burq et al., 2003), and *X. laevis twist* (Hopwood et al., 1989). Primary antibodies used for immunohistochemistry: anti-rabbit phospho-histone H3 (PH3) (BDH, 1:200) or anti-rabbit β-catenin (Sigma, 1:200). Sections were coverslipped with ProLong Gold antifade reagent with DAPI (Invitrogen, P36931).

Confocal Microscopy and Image Analysis

To analyze NC migration, whole-mount E9.0 embryos were cleared using 70% glycerol/PBS and mounted on slides. Sagittal confocal z-stacks were obtained using a Leica TCS SP5 DM16000. Image sequences were reconstructed using Imaris image analysis software. Thickness of NC streams were determined by measuring the depth of GFP positive NC cells at three points anterior to the trigeminal ganglion, posterior to the maxillary compartment (outlined in Figure 3).

μCT

Specimens were scanned using a GE Explore Locus SP μCT scanner. The specimens were immersed in 20% (w/v) Pluronic F-127 (Sigma) at 4°C and warmed to room temperature for immobilization. Specimens were scanned to produce 8 μm voxel size volumes, using an X-ray tube voltage of 80 kVp and a tube current of 80 μA. An aluminum filter (0.05 mm) was used to adjust the energy distribution of the X-ray source. The specimens were characterized further by making three-dimensional isosurfaces, generated and measured using Microview software (GE).

Flow Cytometry of Embryo Heads

Cell purification from embryonic tissues was performed as previously described (Schulz et al., 2012). Heads from *Wnt1-cre;* $R26^{mT/mG}$ embryos, as depicted in Figure 2E, were digested and passed through a 100 μm cell strainer. Flow cytometry was performed using a BD Biosciences FACSAria II cell sorter. Live cells were identified using side scatter and forward scatter (FSC-A), followed by doublet exclusion using forward scatter width against FSC-A. Populations were identified using endogenous expression of GFP and Tomato. All data were analyzed using FlowJo 9.53 (Celeza GmbH).

SUPPLEMENTAL INFORMATION

Supplemental Information includes three figures and can be found with this article online at http://dx.doi.org/10.1016/j.devcel.2013.05.021.

ACKNOWLEDGMENTS

We are grateful to Martyn Cobourne and Marc Dionne for critical reading of the manuscript, Angela Gates and Alasdair Edgar for assistance, the Basson laboratory for help with FGFs, the New Hunt's House Biological Services Unit for excellent animal care, and Albert Basson, Jeremy Green, Paul Sharpe, and Brunella Franco for contributing mouse lines. Work in the Geissmann laboratory (E.G.P. and C.S.) was supported by grants from the Medical Research Council (MRC; G0900867) and the European Research Council (ERC-2010-StG-261299). C.S. was supported by a fellowship from the German National Academy of Sciences Leopoldina (LPDS 2009-31). B.W. and R.H.F. were supported by National Institutes of Health (NIH) grants (ES020619, NS076465, and HD067244). J.B.W. is an Early Career Scientist of the Howard Hughes Medical Institute; work in his laboratory was funded by The March of Dimes and The Burroughs Wellcome Fund. Additional support to J.M.T. was provided by the National Institute of Dental and Craniofacial Research/NIH (F32DE023272). This work was funded by grants to K.J.L. from the Wellcome Trust (WT081880AIA, a Wellcome VIP award for J.M.T., a Wellcome Trust Vacation Studentship for Y.Y.), grants from the Biotechnology and Biological Sciences Research Council (BB/E013872, BB/I021922/1), an MRC studentship (B.Z.Y.), and the King's College London Dental Institute.

Received: August 22, 2012
Revised: March 29, 2013
Accepted: May 23, 2013
Published: June 24, 2013

REFERENCES

Agochukwu, N.B., Solomon, B.D., Doherty, E.S., and Muenke, M. (2012). Palatal and oral manifestations of Muenke syndrome (FGFR3-related craniosynostosis). J. Craniofac. Surg. *23*, 664–668.

Anderson, P.J., Hall, C., Evans, R.D., Harkness, W.J., Hayward, R.D., and Jones, B.M. (1997). The cervical spine in Crouzon syndrome. Spine (Phila Pa 1976) *22*, 402–405.

Aoto, K., Nishimura, T., Eto, K., and Motoyama, J. (2002). Mouse GLI3 regulates Fgf8 expression and apoptosis in the developing neural tube, face, and limb bud. Dev. Biol. *251*, 320–332.

Arts, H.H., Bongers, E.M., Mans, D.A., van Beersum, S.E., Oud, M.M., Bolat, E., Spruijt, L., Cornelissen, E.A., Schuurs-Hoeijmakers, J.H., de Leeuw, N., et al. (2011). C14ORF179 encoding IFT43 is mutated in Sensenbrenner syndrome. J. Med. Genet. *48*, 390–395.

Beales, P.L., Elcioglu, N., Woolf, A.S., Parker, D., and Flinter, F.A. (1999). New criteria for improved diagnosis of Bardet-Biedl syndrome: results of a population survey. J. Med. Genet. *36*, 437–446.

Benadiba, C., Magnani, D., Niquille, M., Morlé, L., Valloton, D., Nawabi, H., Ait-Lounis, A., Otsmane, B., Reith, W., Theil, T., et al. (2012). The ciliogenic transcription factor RFX3 regulates early midline distribution of guidepost neurons required for corpus callosum development. PLoS Genet. *8*, e1002606.

Berkowitz, S. (1971). Stereophotogrammetric analysis of casts of normal and abnormal palates. Am. J. Orthod. *60*, 1–18.

Blaess, S., Corrales, J.D., and Joyner, A.L. (2006). Sonic hedgehog regulates Gli activator and repressor functions with spatial and temporal precision in the mid/hindbrain region. Development *133*, 1799–1809.

Brooks, E.R., and Wallingford, J.B. (2012). Control of vertebrate intraflagellar transport by the planar cell polarity effector Fuz. J. Cell Biol. *198*, 37–45.

Brugmann, S.A., Cordero, D.R., and Helms, J.A. (2010). Craniofacial ciliopathies: A new classification for craniofacial disorders. Am. J. Med. Genet. A. *152A*, 2995–3006.

Chai, Y., and Maxson, R.E., Jr. (2006). Recent advances in craniofacial morphogenesis. Dev. Dyn. *235*, 2353–2375.

Cobourne, M.T., Xavier, G.M., Depew, M., Hagan, L., Sealby, J., Webster, Z., and Sharpe, P.T. (2009). Sonic hedgehog signalling inhibits palatogenesis and arrests tooth development in a mouse model of the nevoid basal cell carcinoma syndrome. Dev. Biol. *331*, 38–49.

Collier, S., and Gubb, D. (1997). Drosophila tissue polarity requires the cell-autonomous activity of the fuzzy gene, which encodes a novel transmembrane protein. Development *124*, 4029–4037.

Cordero, D., Marcucio, R., Hu, D., Gaffield, W., Tapadia, M., and Helms, J.A. (2004). Temporal perturbations in sonic hedgehog signaling elicit the spectrum of holoprosencephaly phenotypes. J. Clin. Invest. *114*, 485–494.

Creuzet, S., Schuler, B., Couly, G., and Le Douarin, N.M. (2004). Reciprocal relationships between Fgf8 and neural crest cells in facial and forebrain development. Proc. Natl. Acad. Sci. USA *101*, 4843–4847.

Danielian, P.S., Muccino, D., Rowitch, D.H., Michael, S.K., and McMahon, A.P. (1998). Modification of gene activity in mouse embryos in utero by a tamoxifen-inducible form of Cre recombinase. Curr. Biol. *8*, 1323–1326.

Endoh-Yamagami, S., Evangelista, M., Wilson, D., Wen, X., Theunissen, J.W., Phamluong, K., Davis, M., Scales, S.J., Solloway, M.J., de Sauvage, F.J., and Peterson, A.S. (2009). The mammalian Cos2 homolog Kif7 plays an essential role in modulating Hh signal transduction during development. Curr. Biol. *19*, 1320–1326.

Fedtsova, N., and Turner, E.E. (2001). Signals from the ventral midline and isthmus regulate the development of Brn3.0-expressing neurons in the midbrain. Mech. Dev. *105*, 129–144.

Ferkol, T.W., and Leigh, M.W. (2012). Ciliopathies: the central role of cilia in a spectrum of pediatric disorders. J. Pediatr. *160*, 366–371.

Ferrante, M.I., Zullo, A., Barra, A., Bimonte, S., Messaddeq, N., Studer, M., Dollé, P., and Franco, B. (2006). Oral-facial-digital type I protein is required for primary cilia formation and left-right axis specification. Nat. Genet. *38*, 112–117.

Firnberg, N., and Neubüser, A. (2002). FGF signaling regulates expression of Tbx2, Erm, Pea3, and Pax3 in the early nasal region. Dev. Biol. *247*, 237–250.

Goetz, S.C., and Anderson, K.V. (2010). The primary cilium: a signalling centre during vertebrate development. Nat. Rev. Genet. *11*, 331–344.

Goodwin, A., Oberoi, S., Landan, M., Charles, C., Groth, J., Martinez, A., Fairley, C., Weiss, L., Tidyman, W., Klein, O., et al. (2012). Craniofacial and dental development in cardio-facio-cutaneous syndrome: the importance of Ras signaling homeostasis. Clin. Genet.

Gray, R.S., Abitua, P.B., Wlodarczyk, B.J., Szabo-Rogers, H.L., Blanchard, O., Lee, I., Weiss, G.S., Liu, K.J., Marcotte, E.M., Wallingford, J.B., and Finnell, R.H. (2009). The planar cell polarity effector Fuz is essential for targeted membrane trafficking, ciliogenesis and mouse embryonic development. Nat. Cell Biol. *11*, 1225–1232.

Gritli-Linde, A., Hallberg, K., Harfe, B.D., Reyahi, A., Kannius-Janson, M., Nilsson, J., Cobourne, M.T., Sharpe, P.T., McMahon, A.P., and Linde, A. (2007). Abnormal hair development and apparent follicular transformation to mammary gland in the absence of hedgehog signaling. Dev. Cell *12*, 99–112.

Hajihosseini, M.K., Wilson, S., De Moerlooze, L., and Dickson, C. (2001). A splicing switch and gain-of-function mutation in FgfR2-IIIc hemizygotes causes Apert/Pfeiffer-syndrome-like phenotypes. Proc. Natl. Acad. Sci. USA *98*, 3855–3860.

Hayward, R., Jones, B., and Dunaway, D. (2004). The Clinical Management of Craniosynostosis (London: MacKeith Press).

Hennekam, R., Allanson, J., and Krantz, I. (2010). Gorlin's Syndromes of the Head and Neck (New York: Oxford University Press).

Heydeck, W., Zeng, H., and Liu, A. (2009). Planar cell polarity effector gene Fuzzy regulates cilia formation and Hedgehog signal transduction in mouse. Dev. Dyn. *238*, 3035–3042.

Hippenmeyer, S., Shneider, N.A., Birchmeier, C., Burden, S.J., Jessell, T.M., and Arber, S. (2002). A role for neuregulin1 signaling in muscle spindle differentiation. Neuron *36*, 1035–1049.

Hong, S.K., and Dawid, I.B. (2009). FGF-dependent left-right asymmetry patterning in zebrafish is mediated by Ier2 and Fibp1. Proc. Natl. Acad. Sci. USA *106*, 2230–2235.

Hopwood, N.D., Pluck, A., and Gurdon, J.B. (1989). A Xenopus mRNA related to Drosophila twist is expressed in response to induction in the mesoderm and the neural crest. Cell *59*, 893–903.

Hosokawa, R., Deng, X., Takamori, K., Xu, X., Urata, M., Bringas, P., Jr., and Chai, Y. (2009). Epithelial-specific requirement of FGFR2 signaling during tooth and palate development. J. Exp. Zoolog. B Mol. Dev. Evol. *312B*, 343–350.

Hu, D., and Helms, J.A. (1999). The role of sonic hedgehog in normal and abnormal craniofacial morphogenesis. Development *126*, 4873–4884.

Huang, X., Goudy, S.L., Ketova, T., Litingtung, Y., and Chiang, C. (2008). Gli3-deficient mice exhibit cleft palate associated with abnormal tongue development. Dev. Dyn. *237*, 3079–3087.

Huber, C., and Cormier-Daire, V. (2012). Ciliary disorder of the skeleton. Am. J. Med. Genet. C. Semin. Med. Genet. *160C*, 165–174.

Ilagan, R., Abu-Issa, R., Brown, D., Yang, Y.P., Jiao, K., Schwartz, R.J., Klingensmith, J., and Meyers, E.N. (2006). Fgf8 is required for anterior heart field development. Development *133*, 2435–2445.

Itoh, N., and Ornitz, D.M. (2011). Fibroblast growth factors: from molecular evolution to roles in development, metabolism and disease. J. Biochem. *149*, 121–130.

Kreiborg, S., and Cohen, M.M., Jr. (1992). The oral manifestations of Apert syndrome. J. Craniofac. Genet. Dev. Biol. *12*, 41–48.

Kreiborg, S., Barr, M., Jr., and Cohen, M.M., Jr. (1992). Cervical spine in the Apert syndrome. Am. J. Med. Genet. *43*, 704–708.

Kuschel, S., Rüther, U., and Theil, T. (2003). A disrupted balance between Bmp/Wnt and Fgf signaling underlies the ventralization of the Gli3 mutant telencephalon. Dev. Biol. *260*, 484–495.

Lai, C.K., Gupta, N., Wen, X., Rangell, L., Chih, B., Peterson, A.S., Bazan, J.F., Li, L., and Scales, S.J. (2011). Functional characterization of putative cilia genes by high-content analysis. Mol. Biol. Cell *22*, 1104–1119.

Lan, Y., and Jiang, R. (2009). Sonic hedgehog signaling regulates reciprocal epithelial-mesenchymal interactions controlling palatal outgrowth. Development *136*, 1387–1396.

Letra, A., de Almeida, A.L., Kaizer, R., Esper, L.A., Sgarbosa, S., and Granjeiro, J.M. (2007). Intraoral features of Apert's syndrome. Oral Surg. Oral Med. Oral Pathol. Oral Radiol. Endod. *103*, e38–e41.

Levin, L.S., Perrin, J.C., Ose, L., Dorst, J.P., Miller, J.D., and McKusick, V.A. (1977). A heritable syndrome of craniosynostosis, short thin hair, dental abnormalities, and short limbs: cranioectodermal dysplasia. J. Pediatr. *90*, 55–61.

Liu, A., Wang, B., and Niswander, L.A. (2005). Mouse intraflagellar transport proteins regulate both the activator and repressor functions of Gli transcription factors. Development *132*, 3103–3111.

Livet, J., Sigrist, M., Stroebel, S., De Paola, V., Price, S.R., Henderson, C.E., Jessell, T.M., and Arber, S. (2002). ETS gene Pea3 controls the central position and terminal arborization of specific motor neuron pools. Neuron *35*, 877–892.

Lorente, C.A., Tassinari, M.S., and Keith, D.A. (1981). The effects of phenytoin on rat development: an animal model system for fetal hydantoin syndrome. Teratology *24*, 169–180.

Mahmood, R., Bresnick, J., Hornbruch, A., Mahony, C., Morton, N., Colquhoun, K., Martin, P., Lumsden, A., Dickson, C., and Mason, I. (1995). A role for FGF-8 in the initiation and maintenance of vertebrate limb bud outgrowth. Curr. Biol. *5*, 797–806.

Martínez-Abadías, N., Percival, C., Aldridge, K., Hill, C.A., Ryan, T., Sirivunnabood, S., Wang, Y., Jabs, E.W., and Richtsmeier, J.T. (2010). Beyond the closed suture in apert syndrome mouse models: evidence of primary effects of FGFR2 signaling on facial shape at birth. Dev. Dyn. *239*, 3058–3071.

Mo, R., Freer, A.M., Zinyk, D.L., Crackower, M.A., Michaud, J., Heng, H.H., Chik, K.W., Shi, X.M., Tsui, L.C., Cheng, S.H., et al. (1997). Specific and redundant functions of Gli2 and Gli3 zinc finger genes in skeletal patterning and development. Development *124*, 113–123.

Monsoro-Burq, A.H., Fletcher, R.B., and Harland, R.M. (2003). Neural crest induction by paraxial mesoderm in Xenopus embryos requires FGF signals. Development *130*, 3111–3124.

Moore, M.H., Lodge, M.L., and Clark, B.E. (1995). Spinal anomalies in Pfeiffer syndrome. Cleft Palate Craniofac. J. *32*, 251–254.

Moore, S.J., Green, J.S., Fan, Y., Bhogal, A.K., Dicks, E., Fernandez, B.A., Stefanelli, M., Murphy, C., Cramer, B.C., Dean, J.C., et al. (2005). Clinical and genetic epidemiology of Bardet-Biedl syndrome in Newfoundland: a 22-year prospective, population-based, cohort study. Am. J. Med. Genet. A. *132*, 352–360.

Muzumdar, M.D., Tasic, B., Miyamichi, K., Li, L., and Luo, L. (2007). A global double-fluorescent Cre reporter mouse. Genesis *45*, 593–605.

Neugebauer, J.M., Amack, J.D., Peterson, A.G., Bisgrove, B.W., and Yost, H.J. (2009). FGF signalling during embryo development regulates cilia length in diverse epithelia. Nature *458*, 651–654.

Noden, D.M. (1975). An analysis of migratory behavior of avian cephalic neural crest cells. Dev. Biol. *42*, 106–130.

Novarino, G., Akizu, N., and Gleeson, J.G. (2011). Modeling human disease in humans: the ciliopathies. Cell *147*, 70–79.

Okada, T., Okumura, Y., Motoyama, J., and Ogawa, M. (2008). FGF8 signaling patterns the telencephalic midline by regulating putative key factors of midline development. Dev. Biol. *320*, 92–101.

Osumi-Yamashita, N., Ninomiya, Y., Doi, H., and Eto, K. (1994). The contribution of both forebrain and midbrain crest cells to the mesenchyme in the frontonasal mass of mouse embryos. Dev. Biol. *164*, 409–419.

Park, T.J., Haigo, S.L., and Wallingford, J.B. (2006). Ciliogenesis defects in embryos lacking inturned or fuzzy function are associated with failure of planar cell polarity and Hedgehog signaling. Nat. Genet. *38*, 303–311.

Peterson, S.J., and Pruzansky, S. (1974). Palatal anomalies in the syndromes of Apert and Crouzon. Cleft Palate J. *11*, 394–403.

Prattichizzo, C., Macca, M., Novelli, V., Giorgio, G., Barra, A., and Franco, B.; Oral-Facial-Digital Type I (OFDI) Collaborative Group. (2008). Mutational spectrum of the oral-facial-digital type I syndrome: a study on a large collection of patients. Hum. Mutat. *29*, 1237–1246.

Raible, F., and Brand, M. (2001). Tight transcriptional control of the ETS domain factors Erm and Pea3 by Fgf signaling during early zebrafish development. Mech. Dev. *107*, 105–117.

Rash, B.G., and Grove, E.A. (2007). Patterning the dorsal telencephalon: a role for sonic hedgehog? J. Neurosci. *27*, 11595–11603.

Rice, R., Spencer-Dene, B., Connor, E.C., Gritli-Linde, A., McMahon, A.P., Dickson, C., Thesleff, I., and Rice, D.P. (2004). Disruption of Fgf10/Fgfr2b-coordinated epithelial-mesenchymal interactions causes cleft palate. J. Clin. Invest. *113*, 1692–1700.

Roehl, H., and Nüsslein-Volhard, C. (2001). Zebrafish pea3 and erm are general targets of FGF8 signaling. Curr. Biol. *11*, 503–507.

Rynearson, R.D. (2000). Case report: orthodontic and dentofacial orthopedic considerations in Apert's syndrome. Angle Orthod. *70*, 247–252.

Schulz, C., Gomez Perdiguero, E., Chorro, L., Szabo-Rogers, H., Cagnard, N., Kierdorf, K., Prinz, M., Wu, B., Jacobsen, S.E., Pollard, J.W., et al. (2012). A lineage of myeloid cells independent of Myb and hematopoietic stem cells. Science *336*, 86–90.

Sensenbrenner, J.A., Dorst, J.P., and Owens, R.P. (1975). New syndrome of skeletal, dental and hair anomalies. Birth Defects Orig. Artic. Ser. *11*, 372–379.

Seo, J.H., Zilber, Y., Babayeva, S., Liu, J., Kyriakopoulos, P., De Marco, P., Merello, E., Capra, V., Gros, P., and Torban, E. (2011). Mutations in the planar cell polarity gene, Fuzzy, are associated with neural tube defects in humans. Hum. Mol. Genet. *20*, 4324–4333.

Singla, V., and Reiter, J.F. (2006). The primary cilium as the cell's antenna: signaling at a sensory organelle. Science *313*, 629–633.

Singla, V., Romaguera-Ros, M., Garcia-Verdugo, J.M., and Reiter, J.F. (2010). Ofd1, a human disease gene, regulates the length and distal structure of centrioles. Dev. Cell *18*, 410–424.

Sive, H.L., Grainger, R.M., and Harland, R.M. (2000). Early Development of *Xenopus laevis*: A Laboratory Manual (Cold Spring Harbor, NY: Cold Spring Harbor Laboratory Press).

Slaney, S.F., Oldridge, M., Hurst, J.A., Moriss-Kay, G.M., Hall, C.M., Poole, M.D., and Wilkie, A.O. (1996). Differential effects of FGFR2 mutations on syndactyly and cleft palate in Apert syndrome. Am. J. Hum. Genet. *58*, 923–932.

Snyder-Warwick, A.K., Perlyn, C.A., Pan, J., Yu, K., Zhang, L., and Ornitz, D.M. (2010). Analysis of a gain-of-function FGFR2 Crouzon mutation provides evidence of loss of function activity in the etiology of cleft palate. Proc. Natl. Acad. Sci. USA *107*, 2515–2520.

Somlo, S., Rutecki, G., Giuffra, L.A., Reeders, S.T., Cugino, A., and Whittier, F.C. (1993). A kindred exhibiting cosegregation of an overlap connective tissue disorder and the chromosome 16 linked form of autosomal dominant polycystic kidney disease. J. Am. Soc. Nephrol. *4*, 1371–1378.

Soriano, P. (1999). Generalized lacZ expression with the ROSA26 Cre reporter strain. Nat. Genet. *21*, 70–71.

Tagliani, M.M., Gomide, M.R., and Carrara, C.F. (2010). Oral-facial-digital syndrome type 1: oral features in 12 patients submitted to clinical and radiographic examination. Cleft Palate Craniofac. J. *47*, 162–166.

Theil, T., Alvarez-Bolado, G., Walter, A., and Rüther, U. (1999). Gli3 is required for Emx gene expression during dorsal telencephalon development. Development *126*, 3561–3571.

Tobin, J.L., Di Franco, M., Eichers, E., May-Simera, H., Garcia, M., Yan, J., Quinlan, R., Justice, M.J., Hennekam, R.C., Briscoe, J., et al. (2008). Inhibition of neural crest migration underlies craniofacial dysmorphology and Hirschsprung's disease in Bardet-Biedl syndrome. Proc. Natl. Acad. Sci. USA *105*, 6714–6719.

Tukachinsky, H., Lopez, L.V., and Salic, A. (2010). A mechanism for vertebrate Hedgehog signaling: recruitment to cilia and dissociation of SuFu-Gli protein complexes. J. Cell Biol. *191*, 415–428.

Ueta, E., Kurome, M., Teshima, Y., Kodama, M., Otsuka, Y., and Naruse, I. (2008). Altered signaling pathway in the dysmorphogenesis of telencephalon in the Gli3 depressed mouse embryo, Pdn/Pdn. Congenit. Anom. (Kyoto) *48*, 74–80.

Vadiati Saberi, B., and Shakoorpour, A. (2011). Apert syndrome: report of a case with emphasis on oral manifestations. J. Dent. (Tehran) *8*, 90–95.

Wen, X., Lai, C.K., Evangelista, M., Hongo, J.A., de Sauvage, F.J., and Scales, S.J. (2010). Kinetics of hedgehog-dependent full-length Gli3 accumulation in primary cilia and subsequent degradation. Mol. Cell. Biol. *30*, 1910–1922.

Wilkie, A.O., Slaney, S.F., Oldridge, M., Poole, M.D., Ashworth, G.J., Hockley, A.D., Hayward, R.D., David, D.J., Pulleyn, L.J., Rutland, P., et al. (1995). Apert syndrome results from localized mutations of FGFR2 and is allelic with Crouzon syndrome. Nat. Genet. *9*, 165–172.

Wilkinson, D.G., Bhatt, S., and McMahon, A.P. (1989). Expression pattern of the FGF-related proto-oncogene int-2 suggests multiple roles in fetal development. Development *105*, 131–136.

Zhang, Z., Wlodarczyk, B.J., Niederreither, K., Venugopalan, S., Florez, S., Finnell, R.H., and Amendt, B.A. (2011). Fuz regulates craniofacial development through tissue specific responses to signaling factors. PLoS ONE *6*, e24608.